Predicting pelvis geometry using a morphometric model with overall anthropometric variables

Journal of Biomechanics 126 (2021) 110633

Contents lists available at ScienceDirect

Journal of Biomechanics

journal homepage: www.elsevier.com/locate/jbiomech

Predicting pelvis geometry using a morphometric model with overall anthropometric variables

Erik Brynskog [a,*], Johan Iraeus [a], Matthew P. Reed [b], Johan Davidsson [a]

[a] Department of Mechanics and Maritime Sciences, Chalmers University of Technology, Gothenburg, Sweden
[b] University of Michigan Transportation Research Institute, Ann Arbor, MI, USA

ARTICLE INFO

Keywords:
Pelvis geometry
Shape variance
Sparse Principal Component Analysis (SPCA)
Multivariate linear regression
Morphometric model

ABSTRACT

Pelvic fractures have been identified as the second most common AIS2+ injury in motor vehicle crashes, with the highest early mortality rate compared to other orthopaedic injuries. Further, the risk is associated with occupant sex, age, stature and body mass index (BMI). In this study, clinical pelvic CT scans from 132 adults (75 females, 57 males) were extracted from a patient database. The population shape variance in pelvis bone geometry was studied by Sparse Principal Component Analysis (SPCA) and a morphometric model was developed by multivariate linear regression using overall anthropometric variables (sex, age, stature, BMI). In the analysis, SPCA identified 15 principal components (PCs) describing 83.6% of the shape variations. Eight of these were significantly captured ($\alpha < 0.05$) by the morphometric model, which predicted 29% of the total variance in pelvis geometry. The overall anthropometric variables were significantly related to geometrical features primarily in the inferior-anterior regions while being unable to significantly capture local sacrum features, shape and position of ASIS and lateral tilt of the iliac wings. In conclusion, a new detailed morphometric model of the pelvis bone demonstrated that overall anthropometric variables account for only 29% of the variance in pelvis geometry. Furthermore, variations in the superior-anterior region of the pelvis, with which the lap belt is intended to interact, were not captured. Depending on the scenario, shape variations not captured by overall anthropometry could have important implications for injury prediction in traffic safety analysis.

1. Introduction

Road traffic injuries are the eighth leading cause of death globally and the leading cause of death in the age-group 5–29 (WHO – Road traffic injuries, 2020). Prevention of these injuries is listed as one of the UN sustainable development goals (UN – SDGs, 2015).

Pelvic bone injuries of occupants in motor vehicle crashes (MVCs) are studied extensively. Pelvic fracture has been identified as the second most common AIS2+ injury in MVCs (Weaver et al., 2013), and the dominating AIS2+ lower extremity injury in lateral and oblique impacts (Pipkorn et al., 2020). For patients with orthopaedic injuries, pelvic ring fractures are associated with the highest early mortality rate and some degree of residual disability can be expected regardless of treatment (Tile et al., 2015). Real-life MVC data has shown that pelvic fracture risk is associated with occupant sex, age, stature and BMI (Melocchi et al., 2010; Schiff et al., 2008; Sochor et al., 2003; Stein et al., 2006; Sunnevång et al., 2015). Considering future autonomous vehicles and seating positions the pelvis injury risk might be accentuated. With the introduction of advanced driver assistance systems, an increased ratio of side impacts on the total number of MVCs is expected (Östling et al., 2019), and consequently an increased ratio of pelvic fractures given current injury data. Furthermore, reclined seating positions creates less beneficial interactions between the pelvis and the lap-belt, increasing the risk for submarining (Rawska et al., 2020).

Pelvic anthropometry, and its involvement in locomotion and posture, is researched extensively using discrete measurements of anatomical landmarks (DelPrete, 2019). Studies have presented detailed 3D morphology of the pelvic bone using Principal Component Analysis (PCA) on e.g. a Belgian population (n = 271) (Audenaert et al., 2019a), a Japanese population (n = 50) (Arand et al., 2018), and a US population (n = 116) (Klein, 2015). However, it is currently unknown to what extent differences in pelvis bone geometry can be linked to risk for injury in MVCs. Recent studies on submarining, using Post Mortem Human Subjects (PMHS), has identified the need to account for subject-specific

* Corresponding author at: Chalmers University of Technology, Department of Mechanics and Maritime Sciences, Vehicle Safety Division, SE-412 96 Gothenburg, Sweden.
E-mail address: erik.brynskog@chalmers.se (E. Brynskog).

https://doi.org/10.1016/j.jbiomech.2021.110633
Accepted 5 July 2021
Available online 24 July 2021

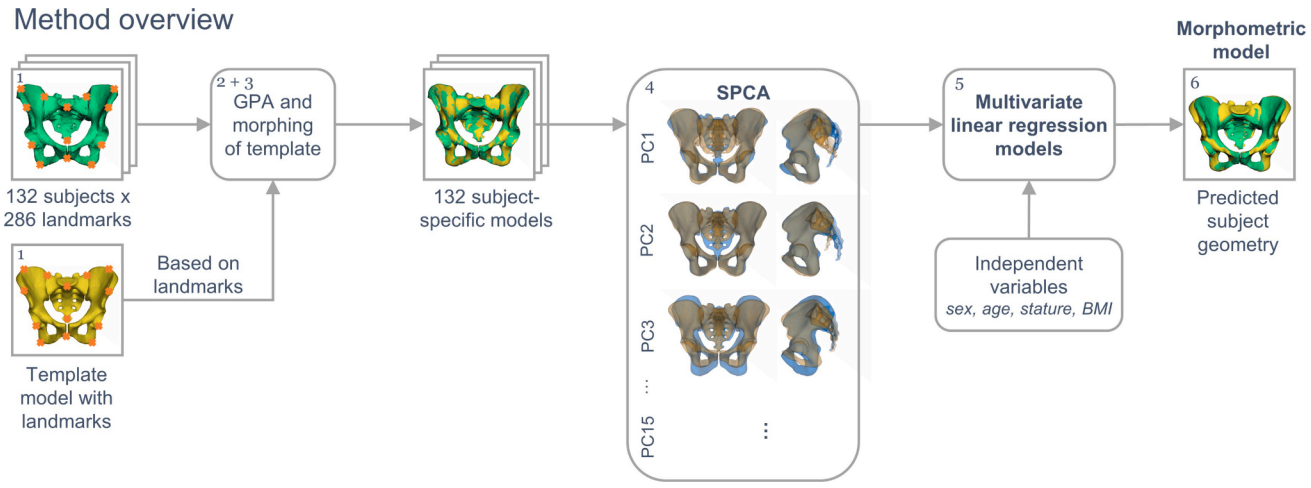

Fig. 1. Schematic overview of study method. (1) Landmark subject geometries and template model, (2) align and scale subject geometries to the template model using GPA on landmarks, (3) morph template model to scaled subject geometries using landmarks to create corresponding node sets, (4) perform SPCA on morphed subject-specific models, (5) perform multivariate linear regression analysis using overall anthropometric variables on GPA and SPCA results, (6) predict subject geometries using morphometric model.

Table 1
Co-variate subject data, mean and 1 S.D., from subjects included in the final morphometric model. As reference, the US population aged 20 years and older have an average stature, weight and BMI of 1.62/1.78 m, 76.4/88.8 kg, and 29.2/28.7 kg/m2, for females/males respectively (Fryar et al., 2016).

	All		Female (n = 74)		Male (n = 56)	
	Mean	S.D.	Mean	S.D.	Mean	S.D.
Age [year]	54.4	20.9	53.7	20.1	55.3	22.1
Stature [m]	1.69	0.11	1.62	0.07	1.79	0.07
Weight [kg]	81.2	21.2	76.3	21.6	87.6	18.9
BMI [kg/m^2]	28.3	6.5	29	7.4	27.4	5.2

factors as pelvic shape and position (Richardson et al., 2020).

Finite Element Human Body Models (FE-HBMs) are used to evaluate occupant injury risk. Using morphing techniques, FE-HBMs can represent a wider portion of the population than those typically used in current injury risk evaluations (Gayzik et al., 2008; Schoell et al., 2015; Shi et al., 2014; Wang et al., 2016; Zhang et al., 2017). Traditionally, linear regression models using overall anthropometry, such as sex, age, stature and BMI, are used to describe the morphing geometries. Results reported on variance captured by these models include 77%/75% for a male/female femur (Klein, 2015), 68%/84% for a male/female tibia (Klein, 2015) and 51% for a ribcage (Wang et al., 2016). However, for the single study on pelvis geometry, such models have so far only captured 15%/18% (male/female) of the total pelvic geometrical variance (Klein, 2015).

Studies of 3D morphology commonly utilize PCA to transform the data and capture most of the shape variance using a smaller set of variables (Slice, 2007). The axes of the transformed system are often referred to as *loading vectors*, while the new variables are called *principal components* (PCs). However, since the PCs are global by nature the result of PCA can be difficult to interpret (Zou et al., 2006). To address this, an extension to PCA called Sparse Principal Component Analysis (SPCA) penalizes the weight of some variables to zero, creating sparse loading vectors that describe localized variance (Zou et al., 2006). Given the complex geometry of the pelvic bone, anatomically localized variations could influence the injury prediction. By knowing which geometrical features that are associated with injury risk for a given scenario we would gain valuable insight into the biomechanics of the system. Studying 2D corpus callosum contours, Sjöstrand et al. (2007) showed that SPCA can extract anatomically meaningful components that are easier to interpret and relate them to clinical data.

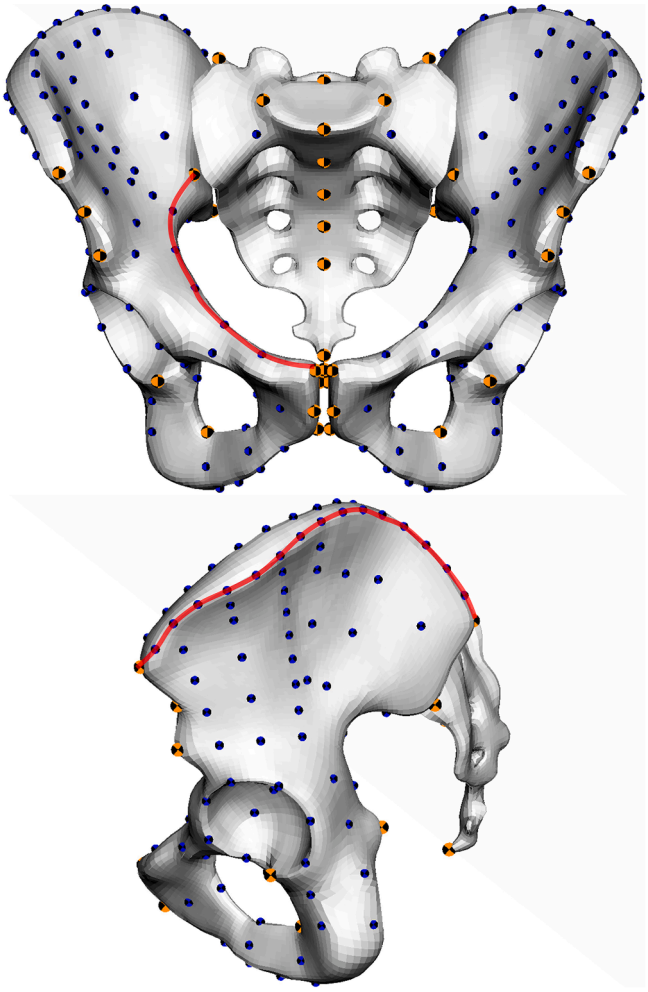

Fig. 2. Position of the anatomical landmarks (n = 286) used for the study. Orange marks fixed anatomical landmarks (n = 38) and blue marks curve semi-landmarks from splines (n = 248). Two splines are shown as example in red. (For interpretation of the references to colour in this figure legend, the reader is referred to the web version of this article.)

Principal Component	Shape Variance Explained	+3 S.D. (blue) and -3 S.D. (orange) of each PC
PC1	31.9%	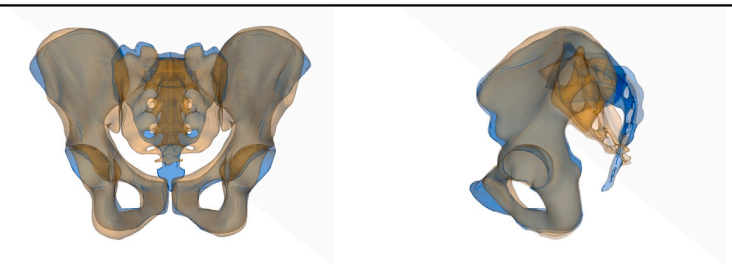 Curvature of sacrum and iliac crest, also some effect on the forward tilt of pubic symphysis
PC2	15.2%	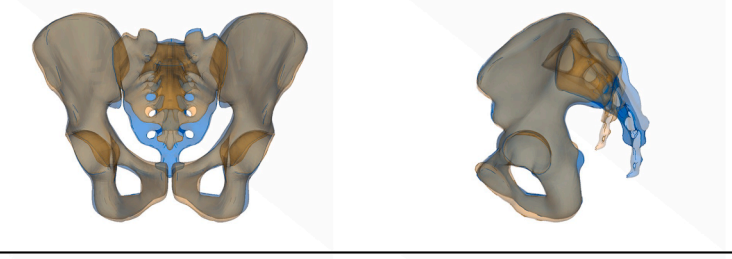 Length of sacrum, also some effect on the pubic symphysis area
PC3	11.5%	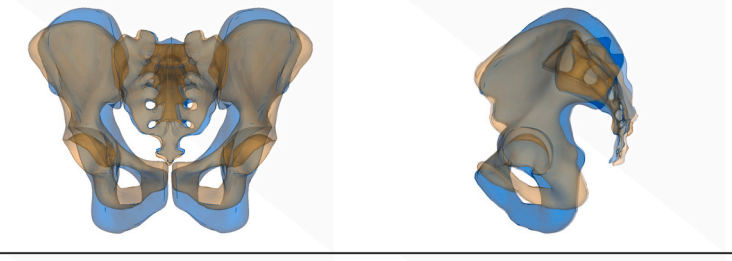 Height of the innominate bone and transverse width of the pelvic inlet
PC4	6.5%	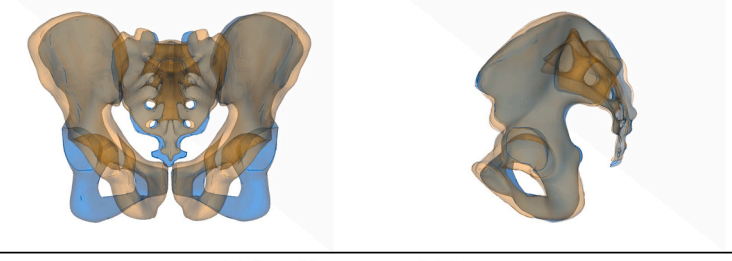 Width of the ischial tuberosities, also some effect on the position of the iliac wings
PC5	4.0%	Rotation of the sacral endplate
PC6	3.2%	Inferior-superior position of sacral endplate (length of superior half of sacrum)
PC7	2.7%	Antero-posterior diameter of the inlet and thickness of pubic bone, some effect on anterior bispinous breadth
PC8	1.7%	Angle between pubic bone and anterior iliac spine, also some effect in iliac spine length
PC9	1.5%	Twist around the vertical axis
PC10	1.2%	Curvature and length of lower sacrum (coccyx)
PC11	1.1%	Posterior bispinous breadth
PC12	0.9%	Size of the iliac wing
PC13	0.8%	Width at acetabulum
PC14	0.8%	Lateral tilt of iliac wings, also some effect on the transverse diameter of the inlet
PC15	0.7%	Inferior position of the ischial tuberosities, also some effect on the anterior bispinous breadth

Fig. 3. Qualitative interpretations of the SPCA results for the first 15 PCs covering 83.6% of the shape variance in the studied population. The first four PCs are visualized at +/− 3 S.D. (blue/orange), while PC5-PC15 are visualized in Appendix B. (For interpretation of the references to colour in this figure legend, the reader is referred to the web version of this article.)

The present study aims to: (1) Describe the shape of the pelvic bones using SPCA, (2) generate an associated morphometric model of the pelvic bones using overall anthropometry as independent variables and (3) identify the local features that are significantly captured by the overall anthropometry. This study will enhance the knowledge of variability in pelvis bone geometry, which can facilitate the development and use of FE-HBMs representing the entire population for assessment of future restraints.

2. Method

Multivariate statistics on dense sets of corresponding nodes, also known as geometric morphometrics (GM) or statistical shape models (SSM) (Slice, 2005), was used to study the population variance in pelvis bone geometries. The steps include; landmarking of subjects and template, registration with Generalized Procrustes Analysis (GPA), morphing of template to each subject geometry using landmarks to create corresponding node sets, performing SPCA on morphed subject-specific

Table 2
Multivariate linear regression models using overall anthropometric variables based on GPA and SPCA results. Coefficients are listed with their corresponding p-value ($\alpha = 0.05$). *p-value from F-statistic to determine if response is significant or non-significant (NS) ($\alpha > 0.05$).

Response	Intercept	Independent variables								p-val.*	Adj. R^2
		Sex [M = 1]	Age [years]	Stature [m]	BMI [kg/m^2]	Sex × Stature	Sex × BMI	Age × BMI	Stature × BMI		
scale	1.823	0.038	−0.001	−0.464	–	–	–	–	–	*<0.001*	**0.48**
		<0.001	*<0.001*	*<0.001*							
PC1	7121.2	549.8	–	−4184.5	−222.3	–	–	–	125.5	*<0.001*	**0.4**
		<0.001		*<0.001*	*<0.01*				*<0.01*		
PC2	–	–	–	–	–	–	–	–	–	*NS*	**–**
PC3	−80.7	−279.3	3.6	–	–	–	–	–	–	*<0.001*	**0.27**
		<0.001	*<0.001*								
PC4	−434.9	662.4	2.7	–	–	–	–	–	–	*<0.001*	**0.65**
		<0.001	*<0.05*								
PC5	5085.3	363.1	3.1	−3144.8	−140.1	–	–	–	80.8	*<0.001*	**0.24**
		<0.001	*<0.05*	*<0.01*	*<0.05*				*<0.05*		
PC6	–	–	–	–	–	–	–	–	–	*NS*	**–**
PC7	4088.8	−1058.7	−2.6	−2387.3	−128	922.5	−22	–	77.5	*<0.001*	**0.17**
		>0.05	*<0.01*	*<0.05*	*<0.05*	*<0.05*	*<0.01*		*<0.05*		
PC8	–	–	–	–	–	–	–	–	–	*NS*	**–**
PC9	–	–	–	–	–	–	–	–	–	*NS*	**–**
PC10	5826.4	385.8	2.5	−3427.5	−214.4	–	–	–	119.8	*<0.001*	**0.47**
		<0.001	*<0.05*	*<0.001*	*<0.001*				*<0.001*		
PC11	−973.8	109.2	1.6	795.7	–	–	–	–	–	*<0.001*	**0.34**
		<0.05	*<0.05*	*<0.05*							
PC12	–	–	–	–	–	–	–	–	–	*NS*	**–**
PC13	–	–	–	–	–	–	–	–	–	*NS*	**–**
PC14	–	–	–	–	–	–	–	–	–	*NS*	**–**
PC15	233.6	251.9	−6.3	–	−13.1	–	–	0.24	–	*<0.001*	**0.47**
		<0.001	*<0.05*		*<0.05*			*<0.05*			

models, and generating a morphometric model using multivariate linear regression to predict the nodal coordinates of the subject-specific models, Fig. 1 describes this process schematically while the following sub-headings describe the details of each step. To create a corresponding representation of each pelvis, a *template model* with a uniform mesh based on the average pelvis geometry was used (see Appendix A for template model development details).

2.1. Description of data

Clinical CT scans were retrospectively obtained (Klein, 2015) from clinical imaging studies at the University of Michigan Department of Radiology through a protocol approved by an institutional review board at the University of Michigan. A radiologist reviewed the studies to ensure that there were no anatomical anomalies or relevant injuries. The scans had an in-plane resolution of 0.625–0.977 mm/pixel, with 1.25 mm between slices. The previous study also segmented the pelvic outer 3D surfaces. Co-variate data for each subject including sex, age, stature, and weight were extracted from medical records for each subject, see TABLE 1. In total, pelvic geometries from 132 adults (75 females, 57 males) were available for this study.

2.2. Landmarking

Landmarks are points representing anatomical structures on a specimen (Slice, 2005) and can be used to align and scale subject geometries to a common reference. Prior to landmarking, each of the subject geometries and the template model were rotated into their standing anatomical position (Reynolds et al., 1982). Using ANSA 20.1.0 (BETA CAE Systems), 286 anatomical landmarks were manually placed on each geometry, where 38 were fixed anatomical landmarks and 248 were curve semi-landmarks defined using splines with equidistant spacing, see Fig. 2. The splines were generated in ANSA by tracing nodes along paths (for example, the lateral iliac crest) or by normal projection (for example on the surface of the iliac fossa). The landmarks were defined with the aim of capturing the subject geometry, by morphing of the template, not in relation to a specific injury location.

2.3. Subject alignment

Subject geometries were aligned and scaled to the template model using Generalized Procrustes Analysis (GPA) on the defined landmarks. GPA retains the geometrical properties that are invariant to location, orientation and scale and has been used extensively in morphometric studies (Slice, 2005). A full GPA was performed (including scaling) since SPCA finds localized geometrical differences and is not appropriate for describing global properties such as size (Sjöstrand et al., 2007). Scale (or centroid size) is defined as the square root of the sum of squared coordinate values in all dimensions and is a descriptor of size for a given set of landmarks (Slice, 2005). GPA was performed using the Matlab function "*procrustes*" (MATLAB R2017b).

2.4. Subject morphing

Morphing the template model into each of the subject geometries was done by using the aligned landmark information as input to a Radial Basis Function with Thin-Plate-Splines (RBF-TPS) interpolation. In short, an RBF takes the form:

$$s(x) = p(x) + \sum_{i=1}^{n} \lambda_i \varphi(\|x - x_i\|) \quad (1)$$

where $p(x)$ is a low order polynomial, λ_i is the weighting coefficient, φ is the basis function, and $\|x - x_i\|$ is the Euclidean distance between x and x_i. In this study, a first-order polynomial for $p(x)$ and the TPS basis function $\varphi(r) = 2r^2\log(r)$ without smoothing was used, where r is the Euclidean distance in 3D. See Hu et al. (2016) for further details.

2.5. Sparse principal component analysis

With a corresponding set of nodes for each subject geometry, SPCA was performed on the nodal coordinates to determine the population variance. SPCA introduces penalty constraints to achieve sparse loading vectors, by formulating the PCA problem as a regression-type optimization problem (Zou et al., 2006). Variable selection techniques from

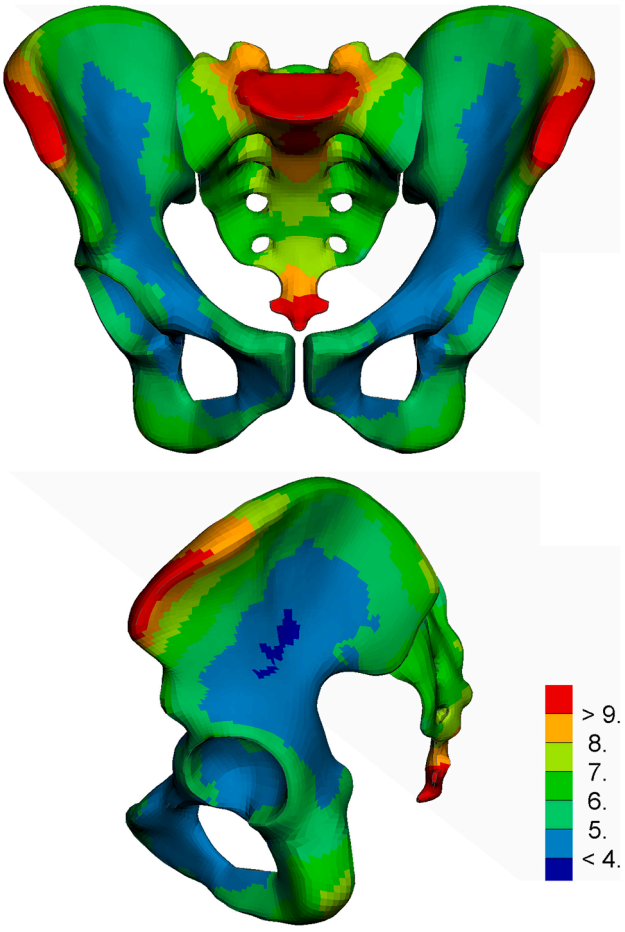

Fig. 4. Median nodal error [mm] for the 130 subjects predicted in 10-fold CV by the morphometric model using overall anthropometry. The error is calculated by comparing the prediction with the subject-specific morphed template model.

multiple linear regression, such as the LASSO or the elastic net, are then integrated into the regression criterion, resulting in PCs with sparse loadings. The general problem formulation can be expressed as:

$$\left(\widehat{\mathbf{A}}, \widehat{\mathbf{B}}\right) = \underset{\mathbf{A},\mathbf{B}}{\operatorname{argmin}} \sum \|\mathbf{X} - \mathbf{A}\mathbf{B}^{\mathrm{T}}\mathbf{X}\|^2 + \psi(\mathbf{B})$$

$$\textit{subject to } \mathbf{A}^{\mathrm{T}}\mathbf{A} = \mathbf{I}, \tag{2}$$

where $\mathbf{B}$ is a sparse weight matrix, $\mathbf{A}$ is an orthonormal matrix and ψ denotes a sparsity inducing regularization such as the LASSO or the elastic net (Zou et al., 2006). The principal components Z are formed as:

$$\mathbf{Z} = \mathbf{X}\mathbf{B} \tag{3}$$

and the original data can be approximately recreated using:

$$\widetilde{\mathbf{X}} = \mathbf{Z}\mathbf{A}^{\mathrm{T}} \tag{4}$$

To solve this optimization problem, the current study utilized a method developed by Erichson et al. (2020), implemented as an R-package "*sparsepca*" (Erichson et al., 2018). The function "rspca" was used with default settings, except maximum number of iterations which was increased from 1,000 to 10,000 to ensure convergence.

2.6. Morphometric model

Similar to previous work (Wang et al., 2016; Weaver et al., 2014), the pelvis bone geometry was separated into two components, scale and shape (described using PC scores). Multiple linear regression models, predicting the nodal coordinates of all surface points (n = 26,024) in the pelvis geometry, were created by relating scale and PC scores to overall anthropometry (sex, age, stature, BMI). Main terms and first order interactions were considered. Bonferroni adjusted p-values on F-statistics were used to exclude shape variations (PCs) not significantly related to the overall anthropometry ($\alpha = 0.05$). Model selection was based on AIC ranking, computed by the "dredge" function from the R-package "MuMIn" (Barton, 2020). For each dependent variable (PC or scale), the highest-ranking model including only significant variables ($\alpha = 0.05$) was selected. Main terms of significant interactions were kept regardless of significance level following the hierarchical principle (James et al., 2017). The final morphometric model predicts a pelvis bone geometry according to Eq. (5):

$$\overrightarrow{\boldsymbol{Subject}_{geom}} = \frac{\overrightarrow{\boldsymbol{Average}_{geom}} + PC1 \times \overrightarrow{\mathbf{PC1}} + PC2 \times \overrightarrow{\mathbf{PC2}} + \cdots + PC15 \times \overrightarrow{\mathbf{PC15}}}{scale} \tag{5}$$

where *scale* and *PC1-PC15* are scalar values predicted using the regression models and $\overrightarrow{\mathbf{PCx}}$ are the loading vectors of each PC from SPCA.

2.7. Morphometric model quality evaluation

Landmarking of six randomly selected subjects (three males and three females) was redone at a later occasion to evaluate intra-observer quality. The Euclidean distance of corresponding fixed anatomical and semi-landmarks, between original and control subjects, was calculated.

Additionally, to evaluate morphing quality, six subject geometries were manually projected to the surface of the morphed geometry using ANSA 20.1.0. The Euclidean distance between the original nodes and the projected nodes was calculated to estimate the deviation.

The variance explained by the morphometric model was evaluated by 10-fold cross-validation (CV). The intercept and slopes were re-calculated for each fold based on 90% of the data while predicting the remaining 10%. Predictability of the morphometric model was evaluated by R^2 as:

$$R^2 = 1 - \frac{SS_{res}}{SS_{tot}}$$

$$SS_{res} = \sum_{i=1}^{n} (y_i - \widehat{y_i})^2 \tag{6}$$

$$SS_{tot} = \sum_{i=1}^{n} (y_i - \overline{y_i})^2$$

where SS_{res} is the residual sum of squares, as calculated by the morphed subject coordinates (y_i) and the predicted subject coordinates ($\widehat{y_i}$), and SS_{tot} is the total sum of squares, as calculated by the morphed subject coordinates and the mean geometry coordinates ($\overline{y_i}$).

For all quality measures, the average median and 90th percentile errors were calculated together with their 95% confidence interval (CI), estimated by a Student's *t*-test.

3. Results

3.1. Landmarks and morphing

The intra-observer quality check of the six tested subjects resulted in a right-skewed distribution of errors. The average median landmark error was 1.4 mm (95% CI ± 0.3 mm), while the average 90th percentile was 2.7 mm (95% CI ± 0.3 mm).

The morphing error, as compared to the original geometries, also resulted in a right-skewed distribution of errors for the six tested subjects. The average median error was 0.7 mm (95% CI ± 0.1 mm), while the average 90th percentile was 2.2 mm (95% CI ± 0.3 mm).

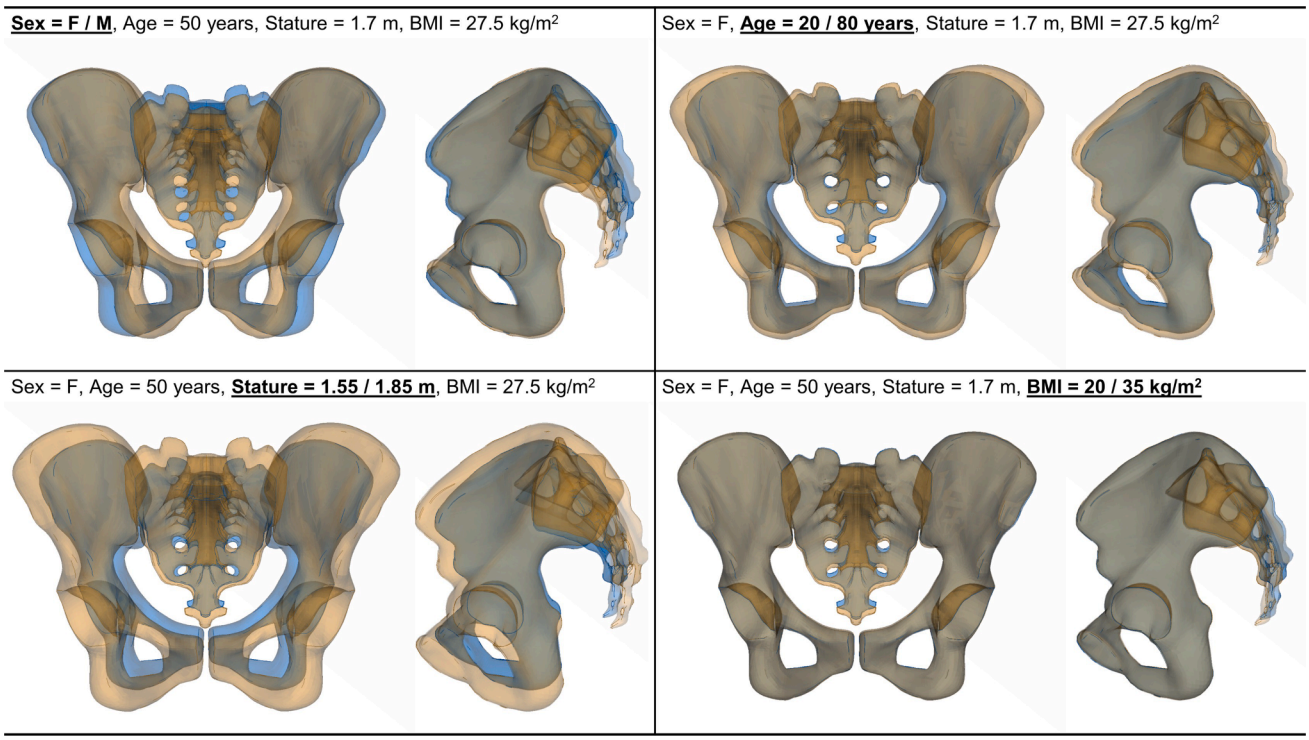

Fig. 5. Effect of changing each of the independent variables while keeping the remaining constant. The first value in blue (reference) and the second value in orange (effect). (For interpretation of the references to colour in this figure legend, the reader is referred to the web version of this article.)

These errors can be compared with the CT in-plane resolution of 0.625–0.977 mm/pixel, with 1.25 mm between slices, and the average shell length of the extracted polygonal geometry of 5.4 mm.

3.2. Analysis of population shape variance

The first 15 PCs captured 83.6% of the shape variance, or 89.8% of the total variance when scaling was included, see Fig. 3, Appendix B and animations in supplementary online material. Substantial variance was found for the shape, position and orientation of sacrum with curvature (PC1 – 31.9%), length (PC2 – 15.2%), rotation of the sacral endplate (PC5 – 4.0%), inferior-superior position of sacral endplate (PC6 – 3.2%), and curvature and length of the lower sacrum (PC10 – 1.2%) covering 55.5% of the variance. Shape variance, not relating to the sacrum, was found for a variety of pelvic dimensions, including pelvic height (superior edge of the iliac crest to the inferior point of the ischial tuberosity in the standing anatomical coordinate system) and transverse width of the pelvic inlet (PC3 – 11.5%) and width of the ischial tuberosities (PC4 – 6.5%). Note that these are qualitative interpretations of the effects of the PCs on the geometry and that the direction of the PC effects is arbitrary.

3.3. Morphometric model

Of the 132 subjects, two were considered outliers and removed from the dataset for the statistical analysis, leaving 130 subjects for the morphometric model. The outliers were a man of 1.52 m stature and a woman of 1.83 m stature with wide and flat hip bones.

The scaling component, PC1, PC3-PC5, PC7, PC10-PC11 and PC15 were significantly related to the overall anthropometric variables. These explained 66.7% of the total variance. TABLE 2 presents the resulting regression models for each response. Evaluating the predictability of the morphometric model for all 130 subjects in 10-fold CV, according to Eq. (6), resulted in an R^2 of 0.29, meaning that the morphometric model captures 29% of the total variance.

The Euclidean nodal error of the predicted models compared to the subject specific models had an average median of 5.8 mm (95% CI ± 0.3 mm) with an average 90th percentile of 10.5 mm (95% CI ± 0.5 mm). The maximum error for any subject was 33.6 mm, found at the tip of the coccyx. Fig. 4 shows the median error of each node for the 130 subjects distributed over the pelvic surface. In general, the overall anthropometric variables were poor predictors of the superior/inferior portion of sacrum and the anterior superior margins of the ilia. The sacrum error was primarily found in the sagittal plane while the main source of anterior superior iliac spine (ASIS) error was found in the lateral direction.

Single variable effects were analysed: female vs male, age 20 vs 80 years, stature 1.55 vs 1.85 m and BMI 20 vs 35 kg/m^2. The morphometric model prediction obtained by changing each variable individually show that sex mainly affects the shape of the inferior-anterior regions, age affects scale and shape along the iliac crest, stature mainly affects scale and BMI has almost no effect on the pelvic bone geometry, see Fig. 5.

The effect of predicting the pelvis geometry of a female/male subject of average stature from the current dataset was also analysed, see Fig. 6. From TABLE 2 one can see that the significant effects included in this prediction are: scale, curvature of sacrum (PC1), pelvic height and transverse diameter of the inlet (PC3), width of the ischial tuberosities (PC4), rotation of the sacral endplate (PC5), antero-posterior diameter of the inlet and thickness of the pubic bones (PC7), curvature and length of lower sacrum (PC10), posterior bispinous breadth (PC11), and inferior position of the ischial tuberosities (PC15).

4. Discussion

In this study, a morphometric model capable of generating population-representative pelvic bone geometries from overall anthropometrics (sex, age, stature, BMI) was developed. The model was based on data from 74 females and 56 males. The ability to predict local geometrical features, as calculated by SPCA, was evaluated. To the

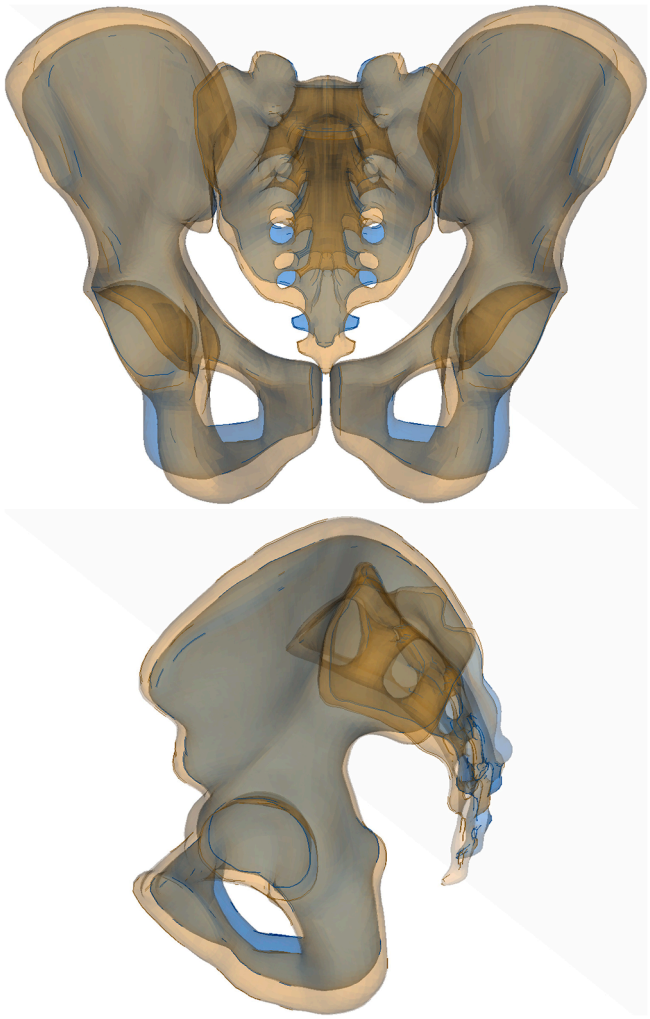

Fig. 6. Predicting an average female of 1.62 m stature (blue) and an average male of 1.79 m stature (orange). (For interpretation of the references to colour in this figure legend, the reader is referred to the web version of this article.)

authors' knowledge, this is the first study to use SPCA to describe the local shape variations of the pelvic bone.

The fact that the morphometric model only account for 29% of the overall variance is an important finding in relation to today's state of the art FE-HBMs which are modelled from CT data of a single subject (Gayzik et al., 2011). The subject represents an average target but given the identified range of variability, and that overall anthropometrics were unable to capture most of the total variance, these single subjects should not be expected to be representative for the pelvis shape. Similar conclusions have been made for the clavicle (Lu and Untaroiu, 2013), the spleen (Yates et al., 2016), and the kidneys (Yates and Untaroiu, 2018). In addition, the developed model enables parametric studies of shape variance to better understand the biomechanical coupling between geometry and risk of injury for different loading scenarios.

4.1. Compared to previous research

Other studies relating to SSMs of the pelvic bones have focused on the anatomical variance (Arand et al., 2018) or on subject-specific 3D geometries based on individual CT data for therapy or pre-operative planning (Audenaert et al., 2019a; Chu et al., 2015; Kainmueller et al., 2009). A previous study using a subset of the current CT dataset developed a regression model of the pelvic bone geometry for population prediction, using age, BMI and bispinous breadth as independent variables for separate male/female models (Klein, 2015). The current study advances that prior work by using an improved landmarking technique, conducting the shape analysis on the entirety of the pelvis mesh rather than just the landmarks, creating a more refined regression model, and by employing SPCA to obtain better interpretability of the PCs with respect to local shape variance.

Compared to models of other skeletal structures using overall anthropometrics as independent variables, the predictability of the pelvic ring is relatively low. Results reported in the literature include 77%/75% for a male/female femur (Klein, 2015), 68%/84% for a male/female tibia (Klein, 2015) and 51% for a ribcage (Wang et al., 2016). The high-scoring models represent geometries that are more one-dimensional, e.g. long bones, with stature accounting for most the predictive strength, while as the geometry includes more dimensional variability the predictability goes down. This suggests that more local variables might be needed to reliably capture the population variance in structures such as the pelvic bone geometry.

4.2. Morphometric model

The current study achieved a predictability of 29% of the population total variance, compared to 15%/18% for male/female pelvic bone models by Klein (2015). In both studies, the predicted model was compared with the subject-specific morphed model, not the subject CT scan. Klein (2015) estimated the mean distance error between observed landmarks and predicted landmarks to 15 mm/17 mm, for the male/female models respectively. For the current study, the average median error of all nodes, measured between subject-specific morphed geometry and predicted geometry, was 5.8 mm.

In this study, a single model was built, instead of separate male/female models, since the interindividual difference was found to be more pronounced than the sex difference with many features overlapping. Combining the two allows for better quantification of how male and female pelves differ than if we were to create two separate models. In addition, splitting the model would not give identical sets of principal components between the two groups. Having one set makes future identification and interpretation of critical shape variations for different injury scenarios easier.

The median nodal error plot presented in Fig. 4 shows that the model best predicted the geometry in the inferior-anterior regions and around the pelvic brim (except the sacral promontory). The strong coupling with sex for these areas partly explains this result (DelPrete, 2019; Luis and Carretero, 1994; Torimitsu et al., 2015). Notably, the anterior superior margins of the ilia and the inferior/superior ends of sacrum showed the largest errors, which was expected since neither of these shape variations were significantly related to overall anthropometry. These variations could have important implications for traffic safety analysis. For example, lap belt engagement with the pelvis could be affected by position and orientation of sacrum/ASIS, and impact timing and force transfer from lateral loading could be affected by the lateral position of the iliac wings relative to the trochanter. The possible coupling between sacrum position/orientation and lap belt engagement can be seen if one considers the attachment with the lumbar spine. If the spine is fixed while e.g. orientation of the sacral endplate is varied, a sagittal tilt of the pelvis that shifts the position of the anterior iliac spine will result.

Single variable effects showed that, see Fig. 5, sex mainly affects the shape of the inferior-anterior regions, age affects scale and shape along the iliac crest, stature mainly affects scale and BMI has almost no effect

on the pelvic bone geometry. Comparing the average female to the average male clear differences were identified, see Fig. 6. As example, significant difference (two-sample *t*-test, $p < 0.001$) was found between the male and female subjects for transverse diameter of the inlet (female mean = 134.1 mm (SD = 10.0), male mean = 127.5 mm (SD = 7.8)), bispinous breadth (female mean = 224.5 mm (SD = 21.3), male mean = 236.8 mm (SD = 18.5)), pelvic height (female mean = 198.5 (SD = 10.2), male mean = 217.6 mm (SD = 10.0)), and sub pubic angle (female mean = 126.1° (SD = 7.6), male mean = 104.7° (SD = 9.2)). However, by studying the total range of variability, see Fig. 3, one can note that interpersonal variation within each sex can be greater than the average difference between sexes.

4.3. Sparse principal component analysis

SPCA was chosen over PCA to achieve PCs with localized shape variations and improved interpretability. However, the need for user-defined solution parameters creates some drawbacks. In the case of PCA, 100% of the variance is always captured and the included level of variance can be decided a posteriori. In SPCA the number of PCs is set a priori and limits the variance captured. Furthermore, the number of PCs included can have some effect on all PCs calculated, not just the added ones. In addition, the sparsity controlling parameter of the solution routine will control the localization and hence affect the shape variations captured. As a result, different settings could affect the shape variations captured and their significance level in the model. There is also a possibility that interesting features could be found in the ~10% of total variance not captured. Building the morphometric model from PCA achieved close to identical predictability indicating that these limitations does not affect the final prediction, only the interpretation of available shape components.

5. Limitations

The data used for this study comes from a single source. Based on overall anthropometry, the sample is representative of a modern US population (Fryar et al., 2016), but further generalization is not possible. This is a typical limitation for similar studies (Arand et al., 2018; Audenaert et al., 2019a).

The SPCA was calculated using the CT scans of all 132 subjects. While this is a relatively large sample size compared with some other studies reporting SSMs of anatomical structures, capturing the tails of the population variance is not guaranteed. Audenaert et al. 2019a built an SSM on 271 subjects for the lower extremities, including the innominate bones of the pelvis but not sacrum. They concluded that population covering descriptive studies should aim to include 200 training samples.

Corresponding node sets for all subjects was achieved by morphing a template model with uniform mesh (n = 26,024) using a smaller set of manually defined landmarks (n = 286). The manual placement limits the repeatability of the study and is a source of uncertainty, as quantified by the intra-observer landmarking error. Automatic methods to achieve a dense correspondence map from CT scans are available and include e.g. segmentation through an SSM (Audenaert et al., 2019b; Chu et al., 2015) or node matching from a template point cloud to a target node set (Lu and Untaroiu, 2013; Yates et al., 2016; Yates and Untaroiu, 2018). Given the varying quality of segmented surfaces, and the complex 3D geometry of the pelvic ring, an automated procedure was deemed unfeasible for the geometries available. A future study could explore the automated methods and use the current model as a starting point.

Declaration of Competing Interest

The authors declare that they have no known competing financial interests or personal relationships that could have appeared to influence the work reported in this paper.

Acknowledgements

This study was financed by Strategic Vehicle Research and Innovation (FFI) (Award number: 2018-04998), by VINNOVA, the Swedish Transport Administration, Swedish Energy Agency, and industrial partners. Partners in the research project are Autoliv, Volvo Cars and Sahlgrenska University Hospital. This work has been carried out in association with SAFER – Vehicle and Traffic Safety Centre at Chalmers, Sweden. The authors would like to thank Jingwen Hu for his insights and sharing of knowledge and code as well as Katelyn Klein and her supervisor Jonathan Rupp for their prior work that led to this study.

Appendix A

An average geometry with a more uniform mesh distribution was developed for a couple of reasons. First, starting from an average geometry will limit the distortion when morphing a future FE model based on the prediction of the morphometric model. Second, the shape variance captured by a specific PC is in relation to how many nodes that are affected. This means that areas with high nodal densities will have greater weight than regions of the geometry with a sparser distribution. A more uniform mesh distribution was targeted to limit this effect.

Fig. A1 describes the process of generating a template model

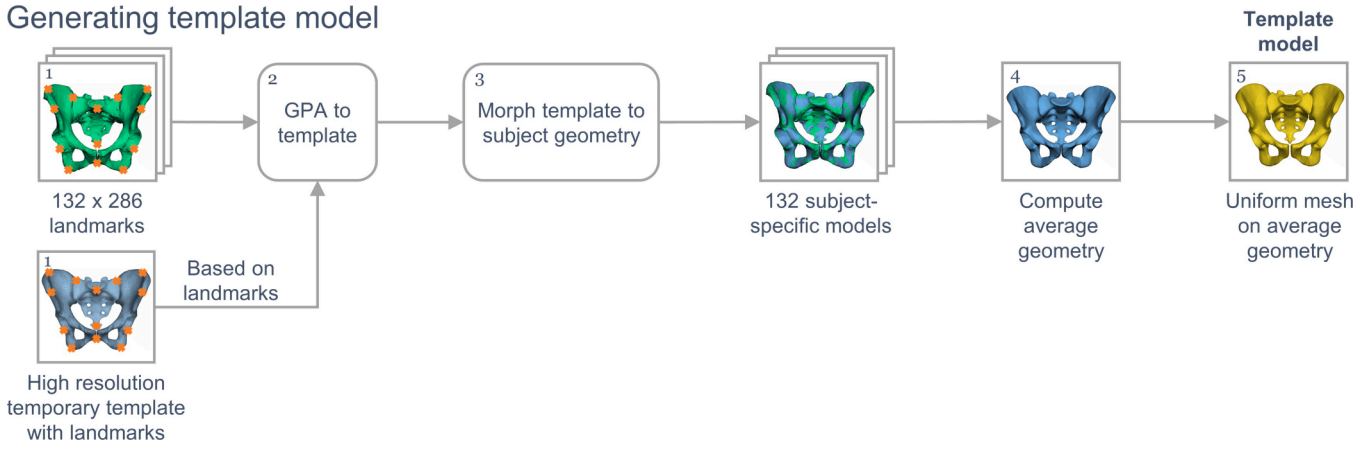

Fig. A1. Schematic overview of template model generation. (1) Landmark subject geometries and temporary template model, (2) align subject geometries to the temporary template model using GPA on landmarks, (3) morph temporary template model to subject geometries using landmarks, (4) compute average geometry from the population, (5) build template model on average geometry by remeshing to a uniform mesh.

schematically. To generate the average geometry a high-resolution file in a polygonal format representing the pelvic bone geometry from a female subject (age 31 years, stature 162 cm, weight 61 kg) was used as a *temporary template*. This geometry was landmarked the same way as the subject geometries. To align the subjects with the temporary template partial GPA was performed (scaling effects excluded). Scaling effects were excluded in this step since the aim was to extract an average-sized geometry rather than study the shape variance. The temporary template was then morphed using RBF-TPS to each subject geometry using the defined landmarks. An average geometry was finally computed as the mean coordinate value for each node. A uniform surface mesh was constructed on the exterior of the average geometry using quad elements with an average element size of 2.5 mm, referred to as the *template model* (total 26,024 nodes).

Appendix B

Resulting PCs from SPCA can be seen in Figs. B1–B3. The shape variations are shown as +/− 3 S.D. and a qualitative interpretation is included.

Principal Component	Shape Variance Explained	+3 S.D. (blue) and -3 S.D. (orange) of each PC
PC1	31.9%	
Curvature of sacrum and iliac crest, also some effect on the forward tilt of pubic symphysis		
PC2	15.2%	
Length of sacrum, also some effect on the pubic symphysis area		
PC3	11.5%	
Height of the innominate bone and transverse width of the pelvic inlet		
PC4	6.5%	
Width of the ischial tuberosities, also some effect on the position of the iliac wings		
PC5	4.0%	
Rotation of the sacral endplate		

Fig. B1. PC1-PC5 from SPCA at +3 S.D. (blue) and -3 S.D. (orange). (For interpretation of the references to colour in this figure legend, the reader is referred to the web version of this article.)

Principal Component	Shape Variance Explained	+3 S.D. (blue) and -3 S.D. (orange) of each PC
PC6 Inferior-superior position of sacral endplate (length of superior half of sacrum)	3.2%	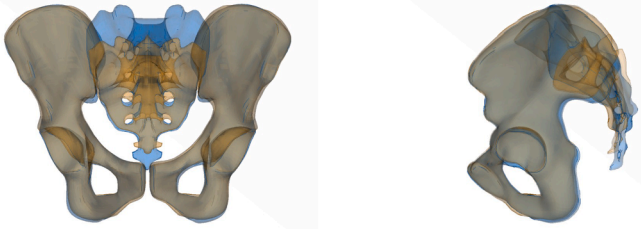
PC7 Antero-posterior diameter of the inlet and thickness of pubic bone, some effect on anterior bispinous breadth	2.7%	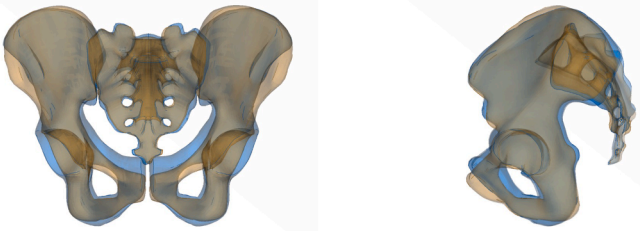
PC8 Angle between pubic bone and anterior iliac spine, also some effect in iliac spine length	1.7%	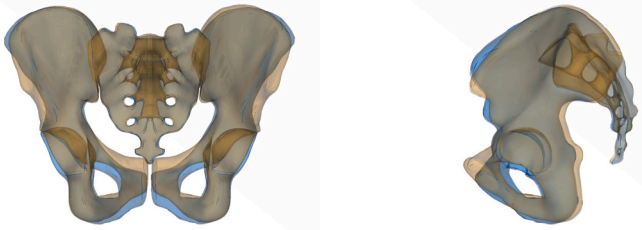
PC9 Twist around the vertical axis	1.5%	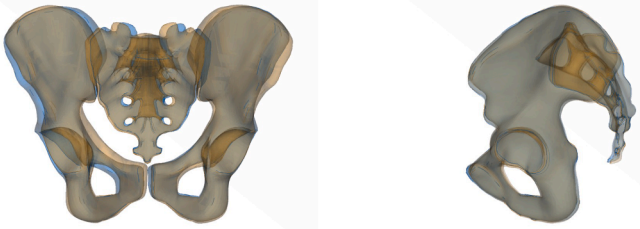
PC10 Curvature and length of lower sacrum (coccyx)	1.2%	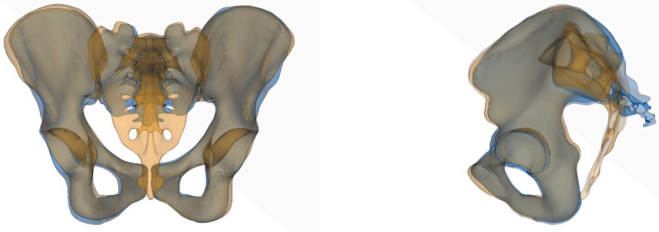

Fig. B2. PC6-PC10 from SPCA at +3 S.D. (blue) and -3 S.D. (orange). (For interpretation of the references to colour in this figure legend, the reader is referred to the web version of this article.)

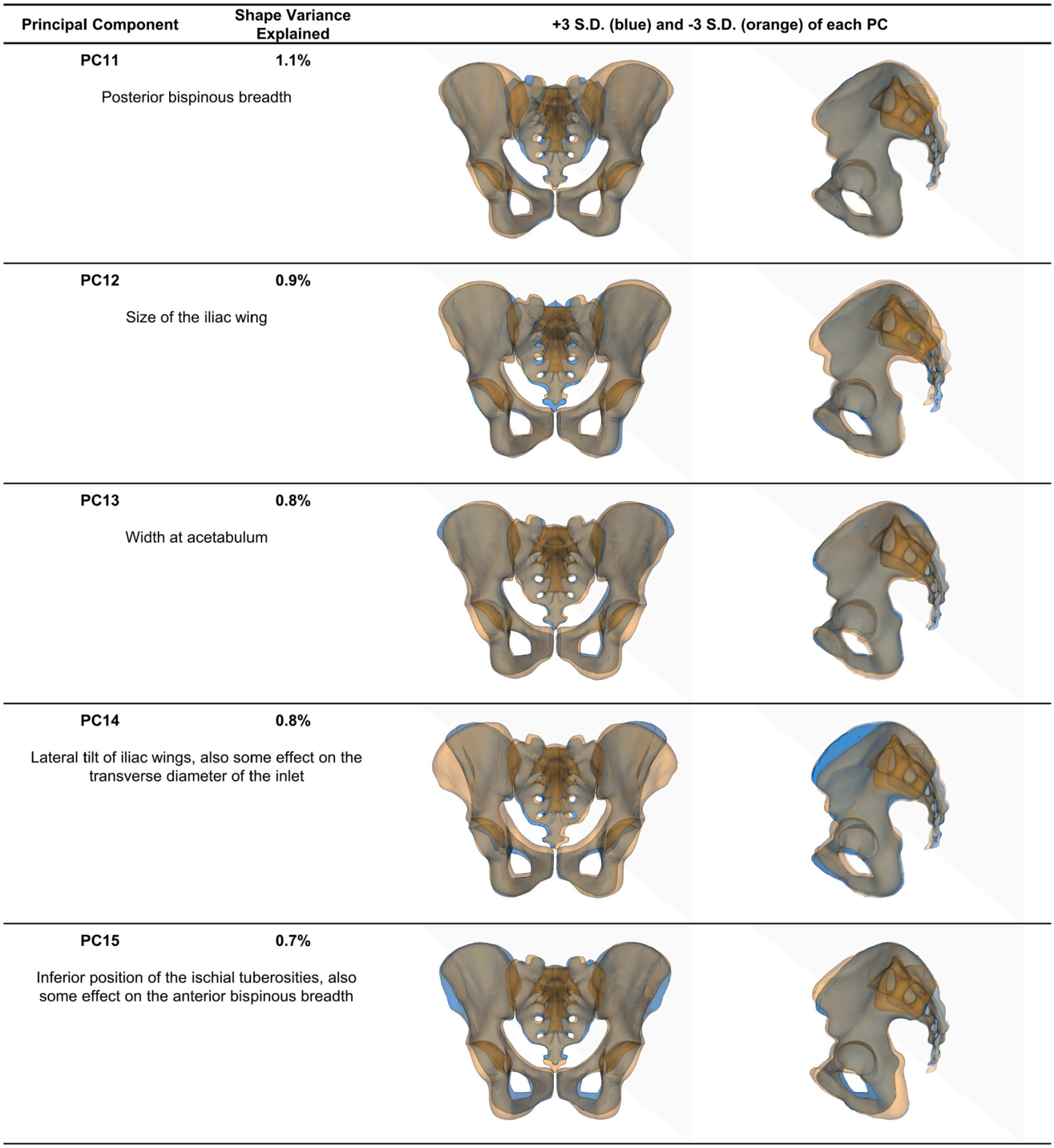

Fig. B3. PC11-PC15 from SPCA at +3 S.D. (blue) and -3 S.D. (orange). (For interpretation of the references to colour in this figure legend, the reader is referred to the web version of this article.)

Appendix C. Supplementary data

Supplementary data to this article can be found online at https://doi.org/10.1016/j.jbiomech.2021.110633.

References

Arand, C., Wagner, D., Richards, R.G., Noser, H., Kamer, L., Sawaguchi, T., Rommens, P. M., 2018. 3D statistical model of the pelvic ring – a CT-based statistical evaluation of anatomical variation. J. Anat. 234, 376–383. https://doi.org/10.1111/joa.12928.

Audenaert, E.A., Pattyn, C., Steenackers, G., De Roeck, J., Vandermeulen, D., Claes, P., 2019a. Statistical Shape Modeling of Skeletal Anatomy for Sex Discrimination: Their Training Size, Sexual Dimorphism, and Asymmetry. Front. Bioeng. Biotechnol. 7, 302. https://doi.org/10.3389/fbioe.2019.00302.

Audenaert, E.A., Van Houcke, J., Almeida, D.F., Paelinck, L., Peiffer, M., Steenackers, G., Vandermeulen, D., 2019b. Cascaded statistical shape model based segmentation of the full lower limb in CT. Comput. Methods Biomech. Biomed. Engin. 22 (6), 644–657. https://doi.org/10.1080/10255842.2019.1577828.

Barton, K., 2020. MuMIn: Multi-Model Inference. R package version 1.43.17. https://cran.r-project.org/package=MuMIn.

Chu, C., Chen, C., Liu, L., Zheng, G., 2015. FACTS: Fully Automatic CT Segmentation of a Hip Joint. Ann. Biomed. Eng. 43 (5), 1247–1259. https://doi.org/10.1007/s10439-014-1176-4.

DelPrete, H., 2019. Similarities in pelvic dimorphisms across populations. Am. J. Hum. Biol. 31 (5) https://doi.org/10.1002/ajhb.v31.510.1002/ajhb.23282.

Erichson, N.B., Zheng, P., Aravkin, S., 2018. sparsepca: Sparse Principal Component Analysis (SPCA). R package version 0.1.2. https://CRAN.R-project.org/package=sparsepca.

Erichson, N.B., Zheng, P., Manohar, K., Brunton, S.L., Kutz, J.N., Aravkin, A.Y., 2020. Spare principal compenent analysis via variable projection. SIAM J. Appl. Math. 80, 977–1002. https://doi.org/10.1137/18M1211350.

Fryar, C.D., Gu, Q., Ogden, C.L., Flegal, K.M., 2016. Anthropometric Reference Data for Children and Adults: United States, 2011-2014, Vital and health statistics. Series 3, Analytical studies.

Gayzik, F.S., Moreno, D.P., Geer, C.P., Wuertzer, S.D., Martin, R.S., Stitzel, J.D., 2011. Development of a full body CAD dataset for computational modeling: A multi-modality approach. Ann. Biomed. Eng. 39 (10), 2568–2583. https://doi.org/10.1007/s10439-011-0359-5.

Gayzik, F.S., Yu, M.M., Danelson, K.A., Slice, D.E., Stitzel, J.D., 2008. Quantification of age-related shape change of the human rib cage through geometric morphometrics. J. Biomech. 41 (7), 1545–1554. https://doi.org/10.1016/j.jbiomech.2008.02.006.

Hu, J., Fanta, A., Neal, M.O.N., Reed, M.P., Wang, J.T.W., 2016. Vehicle crash simulations with morphed GHBMC human models of different stature, BMI, and age. In: Proceedings of the 4th International Digital Human Modeling Conference, Montreal, Canada.

James, G., Witten, D., Hastie, T., Tibshirani, R., 2017. An Introduction to Statistical Learning: with Applications in R, first ed. Springer New York Heidelberg Dordrecht London. https://doi.org/10.1007/978-1-4614-7138-7.

Kainmueller, D., Lamecker, H., Zachow, S., Hege, H.C., 2009. An articulated statistical shape model for accurate hip joint segmentation. In: Proceedings of the Annual International Conference of the IEEE Engineering in Medicine and Biology Society. Minneapolis, MN, pp. 6345–6351. https://doi.org/10.1109/IEMBS.2009.5333269.

Klein, K.F., 2015. Thesis: Use of Parametric Finite Element Models to Investigate Effects of Occupant Characteristics on Lower-Extremity Injuries in Frontal Crashes. University of Michigan. https://deepblue.lib.umich.edu/handle/2027.42/113339.

Lu, Y.-C., Untaroiu, C.D., 2013. Statistical shape analysis of clavicular cortical bone with applications to the development of mean and boundary shape models. Comput. Methods Programs Biomed. 111 (3), 613–628. https://doi.org/10.1016/j.cmpb.2013.05.017.

Luis, J., Carretero, J.M., 1994. Multivariate Analysis of the Sexual Dimorphism of the Hip Bone in a Modern Human Population and in Early Hominids. Am. J. Phys. Anthropol. 93 (2), 241–257.

Melocchi, A.G., Van Horn, M., Faust, D.P., Fowler, G.M., Holcombe, S., Horn, C.K., Joy, K., Kline, A.S., Wang, S., 2010. U of Michigan CIREN Side Impact Field Crashes and Injury Patterns, SAE Technical Paper 2010-01-1157. https://doi.org/10.4271/2010-01-1157.

Östling, M., Jeppsson, H., Lübbe, N., 2019. Predicting crash configurations in passenger car to passenger car crashes to guide the development of future passenger car safety. Proceedings of the IRCOBI Conference.

Pipkorn, B., Iraeus, J., Lindkvist, M., Puthan, P., Bunketorp, O., 2020. Occupant injuries in light passenger vehicles—A NASS study to enable priorities for development of injury prediction capabilities of human body models. Accid. Anal. Prev. 138, 105443. https://doi.org/10.1016/j.aap.2020.105443.

Rawska, K., Gepner, B., Kulkarni, S., Chastain, K., Zhu, J., Richardson, R., Perez-Rapela, D., Forman, J., Kerrigan, J.R., 2020. Submarining sensitivity across varied anthropometry in an autonomous driving system environment. Traffic Inj. Prev. 20 (sup2), S123–S127. https://doi.org/10.1080/15389588.2019.1655734.

Reynolds, H.M., Snow, C.C., Young, J.W., 1982. Spatial Geometry of the Human Pelvis. Federal Aviation Administration Oklahoma City Ok Civil Aeromedical Inst.

Richardson, R., Donlon, J., Jayathirtha, M., Forman, J.L., Shaw, G., Gepner, B., Kerrigan, J.R., Östling, M., Mroz, K., Pipkorn, B., 2020. Kinematic and Injury Response of Reclined PMHS in Frontal Impacts. Stapp Car Crash J. 64, 83–153.

Schiff, M.A., Tencer, A.F., Mack, C.D., 2008. Risk factors for pelvic fractures in lateral impact motor vehicle crashes. Accid. Anal. Prev. 40 (1), 387–391. https://doi.org/10.1016/j.aap.2007.07.005.

Schoell, S.L., Weaver, A.A., Urban, J.E., Jones, D.A., Stitzel, J.D., Hwang, E., Reed, M.P., Rupp, J.D., 2015. Development and Validation of an Older Occupant Finite Element Model of a Mid-Sized Male for Investigation of Age-related Injury Risk. Stapp Car Crash J. 59, 359–383. https://doi.org/https://doi.org/10.4271/2015-22-0014.

Shi, X., Cao, L., Reed, M.P., Rupp, J.D., Hoff, C.N., Hu, J., 2014. A statistical human rib cage geometry model accounting for variations by age, sex, stature and body mass index. J. Biomech. 47 (10), 2277–2285. https://doi.org/10.1016/j.jbiomech.2014.04.045.

Sjöstrand, K., Rostrup, E., Ryberg, C., Larsen, R., Studholme, C., Baezner, H., Ferro, J., Fazekas, F., Pantoni, L., Inzitari, D., Waldemar, G., 2007. Sparse decomposition and modeling of anatomical shape variation. IEEE Trans. Med. Imaging 26 (12), 1625–1635. https://doi.org/10.1109/TMI.2007.898808.

Slice, D.E., 2007. Geometric Morphometrics. Annu. Rev. Anthropol. 36 (1), 261–281. https://doi.org/10.1146/annurev.anthro.34.081804.120613.

Slice, D.E., 2005. Modern Morphometrics in Physical Anthropology. Kluwer Academic / Plenum Publishers, New York.

Sochor, M.R., Faust, D.P., Wang, S.C., Schneider, L.W., 2003. Knee, Thigh and Hip Injury Patterns for Drivers and Right Front Passengers in Frontal Impacts, SAE Technical Paper 2003-01-0164. https://doi.org/https://doi.org/10.4271/2003-01-0164.

Stein, D.M., O'Connor, J.V., Kufera, J.A., Ho, S.M., Dischinger, P.C., Copeland, C.E., Scalea, T.M., 2006. Risk Factors Associated with Pelvic Fractures Sustained in Motor Vehicle Collisions Involving Newer Vehicles. J. Trauma Inj. Infect. Crit. Care 61 (1), 21–31. https://doi.org/10.1097/01.ta.0000222646.46868.cb.

Sunnevång, C., Sui, B.o., Lindkvist, M., Krafft, M., 2015. Census Study of Real-Life Near-Side Crashes with Modern Side Airbag-Equipped Vehicles in the United States. Traffic Inj. Prev. 16 (sup1), S117–S124. https://doi.org/10.1080/15389588.2015.1022895.

Tile, M., Helfet, D.L., Kellam, J.F., Vrahas, M., 2015. Fractures of the Pelvis and Acetabulum – Principles and Methods of Management, 4th ed. Georg Thieme Verlag Stuttgart and Thieme New York.

Torimitsu, S., Makino, Y., Saitoh, H., Sakuma, A., Ishii, N., Yajima, D., Inokuchi, G., Motomura, A., Chiba, F., Yamaguchi, R., Hashimoto, M., Hoshioka, Y., Iwase, H., 2015. Morphometric analysis of sex differences in contemporary Japanese pelves using multidetector computed tomography. Forensic Sci. Int. 257, 530.e1–530.e7. https://doi.org/10.1016/J.FORSCIINT.2015.10.018.

United Nations – Sustainable Development Goals [WWW Document], 2015. URL https://sustainabledevelopment.un.org/sdgs (accessed 6.3.20).

Wang, Y., Cao, L., Bai, Z., Reed, M.P., Rupp, J.D., Hoff, C.N., Hu, J., 2016. A parametric ribcage geometry model accounting for variations among the adult population. J. Biomech. 49 (13), 2791–2798. https://doi.org/10.1016/j.jbiomech.2016.06.020.

Weaver, A.A., Barnard, R.T., Kilgo, P.D., Martin, R.S., Stitzel, J.D., 2013. Mortality-based Quantification of Injury Severity for Frequently Occurring Motor Vehicle Crash Injuries. Ann. Adv. Automot. Med. 57, 235–246.

Weaver, A.A., Schoell, S.L., Nguyen, C.M., Lynch, S.K., Stitzel, J.D., 2014. Morphometric analysis of variation in the sternum with sex and age. J. Morphol. 275 (11), 1284–1299. https://doi.org/10.1002/jmor.20302.

World Health Organization – Road Traffic Injuries [WWW Document], 2020. URL https://www.who.int/news-room/fact-sheets/detail/road-traffic-injuries (accessed 6.3.20).

Yates, K.M., Lu, Y.-C., Untaroiu, C.D., 2016. Statistical shape analysis of the human spleen geometry for probabilistic occupant models. J. Biomech. 49 (9), 1540–1546. https://doi.org/10.1016/j.jbiomech.2016.03.027.

Yates, K.M., Untaroiu, C.D., 2018. Finite element modeling of the human kidney for probabilistic occupant models: Statistical shape analysis and mesh morphing. J. Biomech. 74, 50–56. https://doi.org/10.1016/j.jbiomech.2018.04.016.

Zhang, K., Cao, L., Fanta, A., Reed, M.P., Neal, M., Wang, J.-T., Lin, C.-H., Hu, J., 2017. An automated method to morph finite element whole-body human models with a wide range of stature and body shape for both men and women. J. Biomech. 60, 253–260. https://doi.org/https://doi.org/10.1016/j.jbiomech.2017.06.015.

Zou, H., Hastie, T., Tibshirani, R., 2006. Sparse Principal Component Analysis. J. Comput. Graph. Stat. 15 (2), 265–286. https://doi.org/10.1198/106186006X113430.